LBNL-47348
Preprint

ERNEST ORLANDO LAWRENCE
BERKELEY NATIONAL LABORATORY

Hydrophobic Forces Between Protein Molecules in Aqueous Solutions of Concentrated Electrolyte

R.A. Curtis, C. Steinbrecher, M. Heinemann,
H.W. Blanch, and J.M. Prausnitz

Chemical Sciences Division

January 2001

Submitted to
Biophysical Journal

REFERENCE COPY
Does Not
Circulate
Library Annex Reference
Lawrence Berkeley National Laboratory
Copy 1
LBNL-47348

DISCLAIMER

This document was prepared as an account of work sponsored by the United States Government. While this document is believed to contain correct information, neither the United States Government nor any agency thereof, nor the Regents of the University of California, nor any of their employees, makes any warranty, express or implied, or assumes any legal responsibility for the accuracy, completeness, or usefulness of any information, apparatus, product, or process disclosed, or represents that its use would not infringe privately owned rights. Reference herein to any specific commercial product, process, or service by its trade name, trademark, manufacturer, or otherwise, does not necessarily constitute or imply its endorsement, recommendation, or favoring by the United States Government or any agency thereof, or the Regents of the University of California. The views and opinions of authors expressed herein do not necessarily state or reflect those of the United States Government or any agency thereof or the Regents of the University of California.

LBNL-47348

Hydrophobic Forces Between Protein Molecules in Aqueous Solutions of Concentrated Electrolyte

R. A. Curtis, C. Steinbrecher. M. Heinemann,
H. W. Blanch and J. M. Prausnitz
Department of Chemical Engineering
University of California
and
Chemical Sciences Division
Lawrence Berkeley National Laboratory
University of California
Berkeley, CA 94720, U.S.A.

January 2001

This work was supported by the Director, Office of Science, Office of Basic Energy Sciences, Chemical Sciences Division of the U.S. Department of Energy under Contract Number DE-AC03-76SF00098.

Hydrophobic Forces Between Protein Molecules in Aqueous Solutions of Concentrated Electrolyte

R.A. Curtis, C. Steinbrecher, M. Heinemann, H.W. Blanch, and J.M Prausnitz

Chemical Engineering Department, University of California, Berkeley and

Chemical Sciences Division, Lawrence Berkeley National Laboratory,

Berkeley, CA, 94720, Fax # (510)-643-1228

Keywords: intermolecular interactions, potentials of mean force, lysozyme, salting-out, salts.

Abstract

Protein-protein interactions have been measured for a mutant (D101F) lysozyme and for native lysozyme in concentrated solutions of ammonium-sulfate and sodium-chloride. In the mutant lysozyme, a surface aspartate residue has been replaced with a hydrophobic phenylalanine residue. The protein-protein interactions of D101F lysozyme are more attractive then those of native lysozyme for all experiments. The salt-induced attraction is correlated with the predictions of solvophobic theory where the solvation potential of mean force is given by the work to desolvate the part of the protein surfaces that is buried by the protein-protein interaction. This work is proportional to the aqueous surface-tension increment of the salt and the fractional nonpolar surface coverage of the protein. The experimental measurements are in reasonable agreement with a proposed potential of mean force indicating that the salt-induced attraction between protein

molecules is due to an enhancement of the hydrophobic attraction. This model provides a first approximation for predicting the protein-protein potential of mean force in concentrated aqueous electrolyte solutions, which is useful in determining solution conditions favorable for protein crystallization.

Introduction

Overview

Salt-induced precipitation/crystallization is a common initial step to purify target bio-macromolecules from fermentation broths or crude extracts. Protein crystallization is necessary to obtain protein structures through x-ray diffraction. However, selecting conditions favorable for selective precipitation of a target protein or for obtaining high-quality crystals is difficult because there are a variety of factors that control the thermodynamic and kinetic behavior of protein solutions. Toward a better understanding of these factors, the first step is to determine the effective solvent-averaged protein-protein interactions; these are used to predict properties, such as protein activity coefficients, protein diffusion coefficients, and free energies. However, the interaction between two protein molecules in a solution of concentrated salt is not well understood. Since protein solubility almost always decreases as salt concentration rises, protein-protein interactions become more attractive with increasing salt concentration. Models based on DLVO theory (Verwey and Overbeek, 1948) fail to predict this behavior. The only ionic-strength dependent term in DLVO theory is the electric double-layer potential, which is negligible at the salt concentrations where salting-out is observed. Although protein solubility is a strong function of the type of salt, following the lyotropic series, in

DLVO theory all ions are point charges and the theory does not distinguish between different types of ions of identical charge.

In addition to the forces reflected in the standard DLVO potentials, there are water-mediated forces between protein molecules; these forces are called solvation forces, and include both hydration forces and hydrophobic forces. When the solvent structure adjacent to the protein surface is perturbed, the solvation force is determined by the change in free energy associated with this perturbation (Israelachvili, 1992). Charged or polar surfaces adsorb water molecules; these surfaces are hydrophilic and the forces between them are called hydration forces. Hydration forces are repulsive because as the distance between two hydrated protein molecules decreases, free energy is required to remove the tightly-bound water molecules. Hydrophobic interactions occur between nonpolar protein surfaces; these forces are attractive because as the distance between two nonpolar protein surfaces decreases, the overall free-energy change associated with desolvating nonpolar residues is negative.

In concentrated salt solutions, solvation forces are significantly altered from those in dilute electrolyte solutions because salt ions change the structure of the intervening water (Collins and Washabaugh, 1985). From solubility studies of nonpolar organic solutes, it is known that the hydrophobic interactions between nonpolar residues increase with addition of salt, leading to the well-known salting-out effect (Robinson and Jencks, 1965). Here, we compare protein-protein interactions between native lysozyme molecules with those of a mutant lysozyme as a function of salt type and salt concentration. In the mutated lysozyme molecule, a surface aspartate residue is replaced with hydrophobic phenylalanine. The protein-protein interaction is measured by static

light scattering to determine an osmotic second virial coefficient, B_{22}, that is related to an integral over separation and angles of the potential of mean force (McMillan and Mayer, 1945). The potential of mean force is the free energy of the system when two protein molecules are held at a fixed separation relative to when they are infinitely separated. The results of the comparison are compared with predictions of a simple theory that parallels prediction of the free energy of different conformational states from solvation potentials. As shown in Figure 1, the solvation contribution to the pair potential of mean force is approximated by the reversible work required to desolvate that part of the protein's surface area buried by the interaction. This reversible work is given by the solvation free energy of the buried surface area.

The effect of salt on the solvation free energy of a protein can be related to the predictions of solvophobic theory (Sinanoglu, 1972), where the effect of salt is to increase the surface free energy of nonpolar surface groups (Melander and Horvath, 1977). Because of this, the solvation free energy of the protein in the liquid minus that in the crystal increases with the addition of salt and salting-out occurs (Arakawa and Timasheff, 1985). A second approach to predicting protein phase behavior in the presence of salts uses McMillan-Mayer solution theory, where the thermodynamic properties of the protein solution are solely determined by the free energy of interaction between protein molecules. In applying McMillan-Mayer solution theory to crystal-solution equilibria, it is implicitly assumed that the solvation free energy of the protein in the crystal is identical to that in the liquid. Here, salting-out occurs due to an increase in the solvent-mediated protein-protein attraction with rising salt concentration. By relating protein-protein interactions to predictions of solvophobic theory, we show below that

there is a direct correspondence between McMillan-Mayer theory and the theory of Melander and Horvath.

Solvation Free Energies of Model Compounds

For our purposes here, the protein-protein solvation potential of mean force is given by the free energy required to desolvate the area that is made inaccessible to the solvent due to the interaction. In calculating this free energy it is assumed that (a) the protein surface can be divided into atomic surface groups whose solvation properties are independent of the neighboring groups and (b) the energetics of the solvation of the surface groups is determined by the first hydration layer. Both these assumptions follow from the additivity approximation (Eisenberg and McLachlan, 1986; Hermann, 1972), where the solvation free energy of the entire protein molecule is given by the sum of the solvation free energies of the atomic groups on the protein surface. In our use of the additivity approximation, the desolvation free energy is given by the sum of the surface free energy of each atomic group multiplied by its area buried by the interaction.

The solvation free energy of a solute is equal to the reversible work of "turning on" the intermolecular interactions between the solute and the surrounding solvent molecules (Ben-Naim, 1978), which is equal to the free energy of transferring a solute molecule from an ideal gas to the solvent at a fixed position. The solvation free energies of the atomic groups are determined from a least-squares fitting of model-compound transfer free energies obtained from solubility data. Based on experiments with different-sized hydrocarbons, the solvation free energy for nonpolar molecules is proportional to the area of the solute/solvent interface multiplied by a microscopic surface free energy,

equal to about 25 cal/(mol-Å^2) (Hermann, 1972; Reynolds et al., 1974). Because the solvation free energy is proportional to the solvent-accessible surface area, it is believed that the additivity approximation is valid for predicting nonpolar solvation free energies of proteins (Eisenhaber, 1996).

In solvophobic theory, the solvation free energy is given by the reversible work of forming a molecular interface, which involves the same fundamental forces as the work to form a macroscopic interface. For this reason, the experimentally determined microscopic surface free energy is related to the macroscopic surface tension of the water/hydrocarbon interface, equal to 72 cal/(mol-Å^2). Sharp et al. (1991) have shown that the difference between the experimentally-determined microscopic-surface free energy and the macroscopic surface tension is due to differences in surface curvature, surface roughness, thermal fluctuations, and entropic effects due to mixing unequal-sized spheres in the determination of the microscopic value from solubility data.

The solvation free energy of polar atomic groups is negative due to the favorable electrostatic interaction between the atomic group dipole and water molecules. Because the interaction depends on the dipole moment of the atomic group, there is no universal value for the solvation free energy for different polar groups. Furthermore, because the electrostatic interaction extends more than one hydration layer, there are strong correlations in the solvation of neighboring polar groups. Because of this, the additivity approximation does not necessarily provide an accurate estimate of the solvation free energy of the polar protein surface (Chalikian et al., 1994; Wang and Ben-Naim, 1997).

Solvation Free Energies of Model Compounds in Salt Solutions

The solvation free energy of a model compound in a salt solution can be determined from the salting-out constant. In the absence of solute-solute interactions, the solvation free energy of the solute in the salt solution minus that in salt-free water, termed the water-to-salt transfer free energy, is given by (Ben-Naim, 1978)

$$\frac{G_T}{RT} = -k_s m_3 = \log\left(\frac{S_2}{S_{2,o}}\right) \tag{1}$$

where $S_{2,o}$ and S_2 are the molar solubilities of the solute in pure water and in a salt solution of salt molality, m_3, R is the gas constant, and T is absolute temperature. The salting-out behavior of model nonpolar compounds follows the predictions of solvophobic theory, where the solvation free energy of the solute is proportional to the surface tension of the salt solution, given by

$$\sigma_s = \gamma m_3 + \sigma_o \tag{2}$$

where σ_o and σ_s are the surface tensions of salt-free water and of the salt solution at molality m_3, respectively, and γ is the molal surface-tension increment of the salt. Salting-out experiments have shown that the salting-out constant, k_s, is proportional to γ, where the proportionality constant is similar to the factor needed to correct for the reversible work of forming a microscopic cavity versus a macroscopic interface. Since all salts raise the surface tension of water, nonpolar compounds are always salted-out. The molal surface-tension increment of the salt is correlated with the position of the salt in the lyotropic series, which was originally developed to describe the salting-out effectiveness of various ions for globular proteins (Hofmeister, 1888). For anions, the series is given in decreasing order of the molal surface-tension increment by $SO_4^{2-} > F^- >$

$Cl^- > Br^- > NO_3^- > CLO_4^- > I^- > SCN^-$ and the corresponding series for cations is given by $Mg^{2+} > Na^+ > K^+ > Li^+ > NH_4^+ > Cs^+$. High lyotropic-series salts (kosmotropes) are good salting-out agents because they interact strongly with water; water molecules surrounding the salt ions are more structured relative to bulk water. Low lyotropic-series salts (chaotropes) break the structure of the surrounding water molecules. Chaotropes are weak salting-out agents due to the weak interaction with water.

Studies on the solubilities of model peptides in salt solutions have shown that in addition to the salting-out effect of nonpolar groups, there is a salting-in effect due to an electrostatic interaction between the salt ions and the peptide group. The strength of the interaction generally follows the reverse lyotropic series, however the mechanism of the ion specificity is not clear. Nandi and Robinson (1972) claim that the ion specificity results from an ion-specific interaction whereas the salting-in constant follows a similar order to the Hofmeister series. On the other hand, von Hippel and Schleich (1969) argue that the electrostatic interaction is a non-specific ion-dipole interaction and the apparent specificity results from Hofmeister interactions with nearby nonpolar groups.

Protein-Protein Interactions in Protein Crystallization

George and Wilson (1994) have shown the importance of the pair potential of mean force for predicting solution conditions favorable for protein crystallization; they have shown a B_{22} crystallization window for protein solutions. As a necessary but not sufficient condition for protein crystallization, B_{22} should be in the region -2×10^{-4} and -8×10^{-4} mLmol/g^2. For B_{22} more positive than -2×10^{-4} mLmol/g^2, the protein-protein attraction is usually not sufficiently strong to form stable protein crystals. For solutions

where B_{22} is more negative than -8 x 10^{-4} mLmol/g^2, amorphous precipitation is likely to occur because protein-protein attractions are so strong that the protein molecules do not have adequate time to orient themselves into a crystal lattice. Furthermore, Rosenbaum et al. (1996) have shown that the range of the potential is important for crystallization. For significantly short-ranged potentials, the crystallization window corresponds to a meta-stable liquid-liquid critical point in the vicinity of the liquid-solid equilibrium. This observation is very important for crystallization because density fluctuations are enhanced in the critical region lowering the free energy for formation of critically sized nuclei (ten Wolde and Frenkel, 1997). But unfortunately, the potential of mean force in concentrated salt solutions is not well understood. To take advantage of these crystallization diagnostics, the individual contributions to the total pair potential of mean force (pmf) need to be determined.

Potential of Mean Force Model

The contribution of the solvation pmf to the net protein-protein interaction was described earlier. We use a characteristic surface free energy for nonpolar groups, σ_a, and one for polar groups, σ_p. In addition, we assume the average size of patches of nonpolar and polar surfaces are significantly less than the area buried upon desolvation. With this approximation, the distribution of buried surface groups is uniform and the potential is independent of orientation. The solvation pmf is then given by the probability of overlapping surface groups multiplied by the work to desolvate those surface groups

$$-W_{solv}(r) = A(r)\left(f_a\sigma_a + f_p\sigma_p\right) = A(r)\sigma \qquad (3)$$

where A(r) is the total surface area of the two spheres that is within a surface-surface cut-off separation r_c, for a center-to-center separation, r. From geometric considerations (see Figure 1), A(r) is given by

$$A(r) = \pi d_2^2 - \pi r d_2 + \pi r_c d_2 \tag{4}$$

Here f_a and f_p are the fractional coverages of the nonpolar and polar surface groups, respectively. As r increases, the amount of buried surface area decreases and the magnitude of $W_{solv}(r)$ is given by a monotonically decreasing function that goes to zero at $d_2 + r_c$ where d_2 is the hard-sphere protein diameter. Here, we follow the work of Melander and Horvath (1977) and decompose the surface free energy, σ, into a hypothetical free energy in salt-free water, σ_o, and a term that accounts for the perturbation of the solvation free energy from addition of the salt, given by the first-order correction factor $(d\sigma/dm_3)m_3$.

$$\left(\frac{d\sigma}{dm_3}\right) = f_a \frac{d\sigma_a}{dm_3} + f_p \frac{d\sigma_p}{dm_3} \tag{5}$$

The dependence of the nonpolar solvation free energy on salt concentration, $(d\sigma_a/dm_3)$ is related to the surface-tension increment of the salt by solvophobic theory. In addition to the unfavorable Hofmeister interaction with the nonpolar surface, there are also favorable electrostatic interactions between the salt and the peptide group, whose magnitude follows the reverse lyotropic series. The ion-specific electrostatic interaction is contained in $(d\sigma_p/dm_3)$ and is related to the salting-in constant determined by Nandi and Robinson (1972).

In dilute aqueous electrolyte solutions, the protein-protein interaction has been modeled accurately with DLVO theory where the interaction consists of an electric

double-layer potential, an attractive Hamaker dispersion potential, and a hard-sphere repulsion (Coen et al., 1995; Vilker et al., 1981). When these potentials are incorporated into the pmf model, B_{22} is given by

$$B'_{22} = \frac{2}{3}\pi d_2^3 + \frac{1}{2}\int_{d_2}^{d_2+r_c}\left(1-e^{-\beta W_{solv}}\right)4\pi r^2 dr + \frac{1}{2}\int_{d_2+r_c}^{\infty}\left(1-e^{-\beta W_{DLVO}}\right)4\pi r^2 dr \qquad (6.a)$$

where B'_{22} is related to the experimentally-determined osmotic second virial coefficient B_{22} by

$$B_{22} = \frac{N_{av}B'_{22}}{M_2^2} \qquad (6.b)$$

N_{av} is Avogadro's number and $\beta = (k_B T)^{-1}$ where k_B is Boltzmann's constant. W_{DLVO} is the sum of the electric double-layer repulsion and Hamaker dispersion potentials. The first term is the contribution to B_{22} from protein-excluded volume. The contribution to B_{22} from the solvation potential and from the DLVO potentials are separated by assuming that the solvation potential is significant for short ranges while the DLVO potentials are longer-ranged. The potentials switch at a surface-to-surface separation given by r_c, which is chosen to be approximately one solvent diameter.

Potential of Mean Force Model for Anisotropic Interactions

The effect of salt on the hydrophobic interaction between protein molecules is probed in detail by comparing the results for native lysozyme with that of D101F lysozyme. The difference in the B_{22} values of each molecule is related to an angle-averaged form of the virial coefficient. The angle-dependent solvation free energy of a circular patch mimicing the hydrophobic mutation is given by

$$\Gamma_p(r,\varphi_1,\varphi_2) = -\sigma_a A_p(r,\varphi_1,\varphi_2) \qquad (7)$$

The geometry is shown in Figure 2. A_p is the combined surface area of the two patches that is within a cut-off surface-surface separation, r_c, of the second sphere. φ_1 and φ_2 are the angles of the spheres with respect to the axis connecting their centers that denote the orientation of the patch, and σ_a is the characteristic surface free energy of the nonpolar surface, identical to the corresponding parameter in Eq. 3. The patch is approximated as circular so that the orientation of the patch is independent of rotation about the axis connecting the center of the patch and the center of the sphere. The potential is invariant to rotations of the spheres about the axis connecting the centers of the two spheres, α_1 or α_2. For this case, the angle-averaged potential of mean force is given by

$$e^{-\beta W_p(r)} = \frac{1}{4}\int_0^{\pi} e^{-\beta\Gamma_p(r,\varphi_1,\varphi_2)} \sin(\varphi_1)\sin(\varphi_2)d\varphi_1 d\varphi_2 \tag{8}$$

where the orientation dependence of the buried patch surface area is discussed in Appendix A. The contribution from the patch-patch interaction to B_{22} is

$$B'_{22,D101F} - B'_{22,native} = \frac{1}{2}\int_{d_2}^{d_2+r_c} (1-e^{-\beta W_p(r)})4\pi r^2 dr\,. \tag{9}$$

For strong anisotropic interactions, higher-order interactions are significant at low protein concentrations because the formation of dimers lowers the number of available sites for interaction. For this case, it is more straightforward to use Wertheim's theory of associating fluids (Jackson et al., 1988; Wertheim, 1984). In this model, anisotropic bonds are represented by a site-specific square-well potential given by

$$-\Gamma_p(r,\Omega) = \varepsilon \quad \text{if} \quad r_p < r_c$$

$$-\Gamma_p(r,\Omega) = 0 \quad \text{if} \quad r_p > r_c \tag{10}$$

where r_p is the distance between the patches, r_c is the cut-off separation, Ω is the set of Euler angles denoting the position of the interaction site relative to the center of the molecule, and ε is the interaction free energy between the patches. For relatively weak interactions, the interaction can be related to an osmotic second virial coefficient by integrating the angle-averaged Mayer-f function as in Eq. 8. This is given by

$$\left\langle 1-\exp\left(-\beta\Gamma_p\right)\right\rangle_\Omega = \left(1-\exp\left(\beta\varepsilon\right)\right)\frac{\left(r_c+d_2-r\right)^2\left(2r_c-d_2+r\right)}{6d_2^2 r} \tag{11}$$

The second-virial-coefficient analysis is accurate only for cases when there is a very small fraction of sites involved in bonding. By definition, a site is bonded if there is another site within the cut-off separation of the first. The fraction of sites that are not involved in bonding, X, is given by the equation of mass action

$$X = \frac{-1+\left(1+4\rho_2\Delta\right)^{1/2}}{2\rho_2\Delta} \tag{12}$$

where ρ_2 is the protein number density and Δ is given by

$$\Delta = 4\pi\int g_{ref}(r,\rho_2)\left\langle 1-\exp\left(-\beta\Gamma_p\right)\right\rangle r^2 dr \tag{13}$$

where g_{ref} is the distribution function of the reference system. In the limit of low protein concentrations studied here, g_{ref} can be approximated as unity without significant error. The thermodynamic properties for the associating system have been determined for moderate to high solute densities using thermodynamic perturbation theory. The contribution of the site-site interaction to the Helmholtz energy per protein molecule, a_{int}, is given by

$$\beta a_{int} = \ln X - \frac{X}{2} + \frac{1}{2} \tag{14}$$

The thermodynamic quantities necessary for light-scattering data analysis can be calculated from the appropriate differentiations of Eq. 14.

Experimental Methods

Production of D101F Lysozyme

The mutant lysozyme was produced using the methylotrophic yeast *Pichia pastoris* expression system following the guidelines outlined in the Invitrogen Pichia Expression Kit. The D101F gene was graciously supplied by Prof. J. Kirsch at the University of California at Berkeley. Briefly, the gene was inserted into the pPIC9 expression vector, which contains the DNA coding for the AOX1 promoter and also the *Pichia* wild type gene, HIS4. The constructed vector was cloned into the GS115 wild type strain of *P. pastoris* at the his4 loci from a single crossover event with the HIS4 gene on the vector. The resulting strain of yeast has the same methanol utilization phenotype as the parent strain since the AOX1 gene was kept intact during the insertion of the foreign gene.

The fermentation was performed using a Bioflo III reactor vessel, which was equipped with microprocessor-based PID controllers for pH, temperature, and dissolved oxygen control. The fermentation procedure and medium follows that described by Munshi and Lee (1997). The key aspects of the fermentation protocol include a phase of glycerol excess, a glycerol limited phase, and a ramped MeOH feed phase during the transition from glycerol to methanol feeds. The cell density initially increases in a repressed excess glycerol batch phase. After the glycerol is exhausted, a glycerol feed is initiated at a limiting rate to further increase cell density and to allow derepression of the

AOX1 promoter. The glycerol fed-batch stage is followed by a methanol fed-batch stage where the flowrate of the methanol is slowly increased by 10% every 30 minutes until a maximum feed rate of 10mL/hr·L is obtained. At this time, the fermenter is run in a continuous phase for 24 hours with yields of approximately 100 mg/L D101F lysozyme.

Lysozyme Purification

The fermentation broth was centrifuged at 6000 rpm for 25 min at room temperature to remove cell debris. The supernatant was than loaded on the weak-cation exchange column (500-mL Pharmacia XK-50 column packed with 400 mL of Pharmacia CM Sepharose fast flow resin) at a flow-rate of 10 mL/min and washed with 600 mL of phosphate buffer at a flow rate of 15 mL/min. A glycosylated and un-glycosylated form of D101F lysozyme were eluted into a volume of 350 mL using 0.5 M NaCl solution at a flow-rate of 30 mL/min. The eluent was concentrated and diafiltered using a 200 mL Amicon ultrafiltration unit (YM-3 Amicon membrane with a cut-off of 3000 Da) with three volumes of phosphate buffer. The retentate was then diluted with four volumes of phosphate buffer and loaded on the second column (30 mL Amicon C-30 column packed with Pharmacia SP Sepharose fast flow resin) at a flow-rate of 2 mL/min. The column was washed with 60 mL phosphate buffer at a flow rate of 3 mL/min. The glycosylated form of D101F lysozyme was eluted using 0.18 M NaCl/phosphate buffer at a flow-rate of 3 mL/min and the un-glycosylated form was eluted using the salt solution that was used in the light-scattering experiment or a solution of 0.25 M NaCl, pH 7. The final preparation of the protein required concentrating and washing the eluent with twelve

volumes of the salt solution to be used in the experiment using the 60-mL Amicon ultrafiltration unit (YM-3 Amicon membrane with a cut-off of 3000 Da).

Light Scattering

Light-scattering measurements were made using a Wyatt Technology mini-DAWN static light-scattering detector, which uses a 30-mW semiconductor diode laser at a fixed wavelength of 690 nm. A calibration constant is required to relate the voltage output from the 90° detector to the Rayleigh ratio. However, the calibration constant depends on the solvent because the solid angle that is measured by the detectors depends on the refractive index of the solvent. The instrument software accounts for this effect using known relations between calibration constants and the refractive index of the solvent. The calibration was performed with toluene since it has a known high R_θ.

For each experiment, R_θ was measured for the solvent and for ten to twelve protein samples in order of decreasing concentration. Each sample was pumped through a 0.02 μm Anotop syringe filter at a flowrate of 0.1 mL/min using a Sage-Instruments syringe pump. The lysozyme concentration was measured using a Milton Roy Spectronic 1201 spectrophotometer at a fixed wavelength of 280 nm. A value of 2.635 $cm^3/g{\cdot}cm$ (Sophianopoulus et al., 1962) was used as the extinction coefficient. The lysozyme activity was measured using the Micrococcus lysodeikticus technique (Shugar, 1952) to assure that the protein folded correctly.

Light-Scattering Theory

For the three-component system water (1), protein (2), salt (3) in dilute protein solutions, the light-scattering equation is given by (Stockmayer, 1950)

$$\frac{Kc_2\left(\partial n/\partial c_2\right)^2_{T,\mu_1,\mu_3}}{\overline{R_\theta}} = \frac{1}{RT}\left(\frac{\partial \Pi}{\partial c_2}\right)_{T,\mu_1,\mu_3} \tag{15}$$

where $\overline{R_\theta}$ is the excess Rayleigh scattering of the protein solution over the aqueous salt solution, K is the light-scattering constant, n is the refractive index, c_2 is weight concentration of protein, and Π is the osmotic pressure. Generally, the measurements are made in solutions dilute in protein where only two body interactions are significant. In this case, Eq. 15 reduces to

$$\frac{Kc_2\left(\partial n/\partial c_2\right)^2_{T,\mu_1,\mu_3}}{\overline{R_\theta}} = \frac{1}{M_2} + 2B_{22}c_2 \tag{16}$$

Subsequently, a plot of $Kc_2\left(\partial n/\partial c_2\right)_{T,\mu_1,\mu_3}/\overline{R_\theta}$ vs. c_2 can be used to determine the osmotic second virial coefficient of the protein, B_{22}, and the molecular weight of the protein.

Free-Energy Minimization for D101F

The free-energy minimization of D101F lysozyme was performed using the modules Biopolymer and Discover of the Insight98 software package of Molecular Simulation Inc. Figure 3 shows a space-filling representation of the mutated residue with its surrounding neighborhood along with the same representation of the full molecule. An analogous drawing for the native form is also shown for comparison. The mutated residue sits at the edge of a cleft where it is accessible to the solvent. The accessible

surface areas of the D101F mutant and native lysoyme were calculated with Insight98 using the Michael Connolly Surface package (Connolly, 1993). Results are reported in Table 1.

Results and Discussion

Overview

Infinite-dilution weight-average molecular weights and osmotic second virial coefficients were determined for D101F lysozyme dissolved in solutions of aqueous ammonium sulfate at pH 7 or aqueous sodium chloride with 50-mM sodium acetate buffer, pH 4.5 as a function of salt concentration. The corresponding values for the native form have been reported in Curtis et al. (1998). In all cases, the net interaction between either D101F molecules or native lysoyme molecules becomes more attractive with rising salt molality. The salt-induced protein-protein attractions are correlated with the molal surface-tension increment of the salt. For this reason, the correlations are based on a molality scale instead of the traditional ionic strength scale, which is generally used when electrostatic interactions are the dominant intermolecular forces. The surface-tension increments are 3.11 and 2.36 cal/molA^2-kg/mole for ammonium sulfate and for sodium chloride, respectively. In all regressions of the light-scattering data, the surface free-energy parameters are regressed from the data holding all other parameters fixed as listed in Table 1.

Protein-Protein Interactions of Native Lysozyme Molecules

Figure 4 shows B_{22} for native lysozyme in solutions of sodium chloride or ammonium sulfate plotted versus salt molality. Because lysozyme solubility follows the reverse lyotropic series with respect to the anion, it is expected that the protein-protein interactions are more attractive in sodium chloride than in ammonium sulfate. The abnormal solubility behavior is attributed to changes in the protein-protein interactions upon anion binding to the positively-charged protein surface. Interactions between lysozyme-chaotropic anion complexes are more attractive then those between uncomplexed lysozyme molecules (Ries-Kautt and Ducruix, 1989), whereas the opposite behavior is observed for the interactions between lysozyme-kosmotropic anion complexes (Curtis et al., 1998). However, the effect of ion binding on the protein-protein interactions should not be significant for the conditions studied here. The experiments in ammonium sulfate solutions are at pH 7 where insignificant sulfate ion binding occurs because lysozyme has a low net positive charge at this pH. In the sodium-chloride solutions, since the slightly chaotropic chloride ion binds to the slightly chaotropic imidazolium ion, the protein surface chemistry is not significantly altered; consequently the protein-protein interactions do not change upon chloride-ion binding. Here, the protein-protein interactions in sodium chloride are slightly more attractive than those in ammonium sulfate if compared at constant ionic strength, while the opposite is true if the intermolecular interactions are compared at the same molality. When compared on the molality scale, it is expected that the protein-protein interactions in ammonium sulfate are more attractive than those in sodium chloride because ammonium sulfate has a larger molal surface-tension increment.

The surface free-energy parameter, σ, is fit to the values of B_{22} using the pmf model described by Eq. 6. The extrapolation of σ to zero salt molality in Figure 5 yields a characteristic surface free energy in salt-free water, σ_o, of approximately 6 cal/molÅ^2. This result is independent of the type of salt, as shown by the data; σ_o should also be independent of pH since the electrostatic interactions are incorporated in the pmf model separately with the electric double-layer repulsion potential. The slope of the plot is related to the effect of salt on the solvation free energy of the protein. Generally the salting-out constant is significantly greater than that for salting-in and the effect of salt on the polar surface can be neglected as a first approximation. Subsequently, Eq. 5 reduces to

$$\frac{d\sigma}{dm_3} = f_a \frac{d\sigma_a}{dm_3} = 0.49 \frac{d\sigma_a}{dm_3} \tag{17}$$

The fractional nonpolar surface coverage, f_a, is given by the fractional coverage of carbon atoms as reported in Table 1. The derivative $d\sigma_a/dm_3$ can be calculated from Eq. 17 and Figure 5. The ratio of $d\sigma_a/dm_3$ to the molal surface-tension increment is 1.1 for ammonium sulfate and for sodium chloride. As discussed earlier, solvophobic theory predicts that this ratio is on the order of a third due to the difference in the reversible work of forming a microscopic cavity and of forming a macroscopic interface. This result has only been shown from salting-out experiments on small organic compounds. Subsequently, it is not clear whether the protein surface should be treated as a microscopic cavity or a macroscopic interface. From preferential interaction-parameter measurements, Arakawa and Timasheff (1984) obtained 0.684 for the ratio of the measured surface free-energy increment versus that predicted using solvophobic theory

without correcting for the work of forming a microscopic cavity. In addition, Arakawa and Timasheff (1984) assumed that the entire protein surface contributes to the nonpolar/water interfacial area. If only the non-polar surface is included in the calculation of the interfacial area, the ratio is 1.3, in agreement with our result.

D101F Lysozyme in Solutions of Sodium Chloride

Osmotic second virial coefficients for D101F lysozyme are compared to those of native lysozyme in Figure 6. The difference in B_{22} is determined by the hydrophobic interactions of the mutated residue. As the salt concentration rises, the surface free energy of the nonpolar patch increases and the attraction is enhanced. The contribution to the potential of mean force from the mutation is determined by our model for the patch-patch interaction or by using Wertheim's theory of associating fluids. In the latter theory, the mutation is modeled as a point and the potential is given by a square-well potential. Because the site does not have a finite surface area, it is impossible to determine a surface free energy from the potential without making an assumption about the buried surface area that corresponds to the interaction. Since the interaction is given by a square well, the buried surface area must remain constant for all separations. Here it is assumed that the residue is totally buried over the width of the square well. The model for the patch-patch interaction is more realistic because the mutated residue has a finite surface area and subsequently the amount of surface buried by the interaction depends on the separation. Wertheim's theory is used to model higher-order interactions that become significant at low protein concentrations for strong anisotropic interactions. In Figure 7, the predictions of Wertheim's model are compared to that of the osmotic virial expansion

truncated at the second virial coefficient. The interaction strength is typical of results obtained by fitting the patch-patch interaction to data for concentrated sodium-chloride solutions. The slight positive deviations from two-body interactions are due to a small amount of association (as shown in the inset of Figure 7), which reduces the number of available sites for interaction. This effect is not included in the model for the patch-patch interaction. For the sodium-chloride solutions, we expect that the results of the patch-patch model are more accurate because the contributions from higher-order interactions are small.

Figure 8 shows the results of fitting the nonpolar surface free-energy parameter, σ_a, using the patch-patch interaction model or Wertheim's site-site interaction model for sodium-chloride solutions. In all cases, the values of σ_a fit to the patch-patch model are greater than those of Wertheim's model, indicating the area of interaction integrated over surface-to-surface separation is greater for Wertheim's model. The extrapolated nonpolar surface free energy in salt-free water of 30.5 cal/molÅ^2 is slightly larger than the currently accepted 18 cal/molÅ^2 (Eisenhaber, 1996), although results from studies have ranged from 16 to 33 cal/molÅ^2. The slope of the plot, $d\sigma_a/dm_3$, is equal to 3.6 cal/molÅ^2-kg/mole, slightly larger than the surface-tension increment of sodium chloride. This result is also similar to that obtained by fitting B_{22} to the uniform solvation pmf model, where the nonpolar surface is dispersed in small patches, in contrast to the large continuous patch due to the mutation. The close agreement of the nonpolar surface-free-energy increments obtained by either method indicates that the additivity approximation is valid for the hydrophobic interaction in salt solutions. This agreement provides support that the range of the interaction is on the order of a solvent diameter. The

difference in the increments may be attributed to the favorable interaction between the salt and the polar surface, which needs to be included in the calculation of the total surface free-energy increment given by Eq. 7.

Here, we find that the nonpolar surface free energy in salt-free water is described using a microscopic cavity because this measured surface free energy is on the order of those values reported for small nonpolar compounds. This is in contrast to the result obtained from correlating the effect of salt on the hydophobic interaction where the protein surface is considered as a macroscopic interface.

Apparent Molecular Weights of D101F Lysozyme

Figure 9 gives the apparent molecular weights for D101F lysozyme in solutions of ammonium sulfate or sodium chloride. The experimental results assymptotically approach 16,000 g/mol, greater than the molecular weight of the monomer, 14,600 g/mol, indicating that there is either a small degree of pre-aggregation or a high-molecular-weight impurity in all the solutions. High-molecular-weight impurities were not detected in SDS-gel electrophoresis; it is therefore more likely that there is a small degree of irreversible aggregation. The irreversible aggregation is not expected to influence the results because the fraction of pre-aggregation is small. For the solutions in concentrated ammonium sulfate, the large apparent molecular weights indicate that there is strong association at low protein concentrations. The association is undetectable because the sensitivity of the experiment is too low to measure accurately data at protein concentrations less than 1 g/L for solutions of lysozyme.

D101F Lysozyme in Solutions of Ammonium Sulfate

Figure 10 gives measured second virial coefficients for native and D101F lysozyme. At low salt concentration, the difference in B_{22} is related to the patch-patch interaction. As salt concentration rises, the difference decreases because the anisotropic patch-patch interaction is saturated at low protein concentration as observed from the large apparent molecular weight. Because higher-order interactions are not incorporated in the patch-patch model, we only use Wertheim's model to analyze the data for lysozyme in ammonium-sulfate solutions.

The data fit for Wertheim's model is presented in Figure 11 for D101F lysozyme dissolved in 1.0 molal ammonium-sulfate solution. Here, the curvature is over-predicted for the range of lower protein concentrations, observed for all experiments in ammonium sulfate solutions. It is not clear whether the error is due to an over-simplification of the protein-protein interactions or to a systematic error from the lack of sensitivity of the light-scattering detector. The protein may form aggregates that do not dissociate at infintely-dilute protein concentrations. However, these aggregates are not irreversible because dialyzing the solutions to lower salt concentration leads to dissociation of the aggregates. Figure 12 shows the result of regressing the nonpolar surface free energy, σ_a. The value of σ_a at zero salt molality is 36 cal/molÅ^2. According to the results in sodium-chloride solutions, Wertheim's model under-predicts σ_a by 5 cal/molÅ^2 with respect to the more realistic patch-patch interaction model. If this correction is included, the salt-free value of σ_a is approximately 41 cal/molÅ^2, significantly greater than the corresponding value obtained from the data in sodium-chloride solutions. Despite the inaccuracy of

Wertheim's model, the ratio of the regressed nonpolar surface free-energy increment to the surface-tension increment is 1.9, in good agreement with 2.2, obtained from data for sodium-chloride solutions.

Conclusions

We have compared protein-protein interactions between native lysozyme molecules with those of mutant lysozyme molecules as a function of salt type and salt concentration. A surface aspartate residue is replaced with a hydrophobic phenylalanine group in the mutated lysozyme molecule. The difference in the protein-protein interactions of the native lysozyme molecules and those of the mutant molecules indicates that the hydrophobic interaction is enhanced with addition of salt or by increasing the lyotropicity of the salt.

We have shown that salting-out of proteins can be explained in terms of the effect of salt on the water-mediated forces between protein molecules. The solvation force is approximated by the surface area that is made inaccessible to the solvent by the interaction, multiplied by the negative of an average surface free energy of the nonpolar and polar surface groups. Addition of salt promotes the formation of protein-protein attractions by increasing the surface free energy of the nonpolar groups according to the molal surface-tension increment of the salt. The effect of salt on the solvation of the polar groups is less pronounced, although a slight salting-in effect is observed when comparing the results obtained for solutions of sodium chloride versus those of ammonium sulfate. This model is not new; it is similar to the salting-out theory of Melander and Horvath (1977) and also Arakawa and Timasheff (1985), where protein

solubility was determined from the reduction in unfavorable solvation free energy upon transferring a protein molecule from solution to crystal. Most recent work on predicting protein phase diagrams has used McMillan-Mayer theory, where the thermodynamic properties of the protein solutions are determined by solvent-mediated protein-protein interactions. We have shown that solvent-mediated protein-protein interactions can be explained in terms of the effect of salt on the nonpolar surface free energy of the protein, providing the connection between models based on McMillan-Mayer theory and those originating from the work of Melander and Horvath.

The model presented here is based on the assumption of additivity in the solvation properties of the nonpolar or polar groups. This assumption is known to be in error for polar groups. From our results, the effect of salt on the solvation force is mainly given by changes in hydrophobic interactions. Consequently, the error introduced by assuming additivity only affects the extrapolated surface free energy at zero salt molality. Recent work has shown that protein-protein interactions under crystallizing conditions are accurately modeled using an adhesive potential (Rosenbaum et al., 1996). Subsequently, we conclude that the dominant protein-protein interactions are short-ranged, consistent with the salt-mediated hydrophobic interactions given here.

Appendix A: Calculation of the Area of Patch Buried during Protein-Protein Interaction

The effect of the mutation on protein-protein interactions is included in the model by placing circular hydrophobic patches on the surfaces of the spheres. The two-body potential is given by the combined area contained on the patches that is within a

separation, r_c, of the opposing sphere multiplied by the negative of the nonpolar surface free energy. The interaction is referred to as the patch-patch interaction, although the interaction includes all configurations where either patch is at least partially desolvated. Subsequently, non-local interactions of a patch and the uniform surface are also included in the overall potential.

In this appendix, the area of a patch within a separation, r_c of a second sphere, is calculated. According to Figure 2, the area needs to be determined as a function of φ_1. The calculation is diagrammed in Figure 13. The area is determined by calculating the common arc length between the patch and concentric circles, which are everywhere equidistant from the opposing sphere. The concentric circles are given by the dashed lines in Figure 13. Integration of the common arc lengths to the cut-off separation gives the buried surface area.

The centers of the concentric circles are at a distance x_o from the center of the spheres in which they are contained, and a distance of $r - 2x_o$ from the opposing sphere. The radii, h, are given by the chord theorem

$$h(x_o) = \left[(R + x_o)(R - x_o)\right]^{1/2} \tag{A.1}$$

Subscripts o refer to the coordinates of the concentric circles. The patch is approximated as circular with an area given by the surface area calculated from the crystal structure given in Table 1. The solid angle of the patch, θ, is determined from fitting the area of the patch, A_p

$$A_p = 2\pi R^2 \int_0^{\theta} \sin\theta' d\theta' \tag{A.2}$$

The projected radius of the patch, R_p, is

$$R_p = R\sin\theta \tag{A.3}$$

The equation of the boundary of the patch needs to be determined to calculate the intersection of the patch with the concentric circles. The equation for the boundary of the patch is given by

$$y_p'^2 + z_p'^2 = R_p^2 \tag{A.4}$$

Subscripts p refer to the coordinates of the boundary of the patch. The coordinate transformation is calculated from the matrix, C, for a rotation given by φ_1

$$C = \begin{vmatrix} \cos\varphi_1 & \sin\varphi_1 & 0 \\ -\sin\varphi_1 & \cos\varphi_1 & 0 \\ 0 & 0 & 1 \end{vmatrix} \tag{A.5}$$

where

$$\begin{vmatrix} x' \\ y' \\ z' \end{vmatrix} = C \begin{vmatrix} x \\ y \\ z \end{vmatrix} \tag{A.6}$$

The corresponding equation for the boundary of the patch in the x,y,z coordinate system is calculated from Equations A.5 and A.3.

$$\left[y_p\cos\varphi_1 - x_p\sin\varphi_1\right]^2 + z_p^2 = R_p^2 \tag{A.7}$$

The equation for the concentric spheres as a function of x is

$$y_o^2 + z_o^2 = h^2 = (R - x_o)(R + x_o) \tag{A.8}$$

Equation A.6 and A.7 are solved simultaneously for the intersection of the concentric circles with the boundary of the patch as a function of x. The arc-length, δ, common to the circle and the patch is determined from the points of intersection given by z_i and y_i.

$$\delta(x) = 2h(x)\arctan\left|\frac{z_i(x)}{y_i(x)}\right| \qquad \text{if } y_i > 0$$

$$\delta(x) = 2h(x)\left[\pi - \arctan\left|\frac{z_i(x)}{y_i(x)}\right|\right] \qquad \text{if } y_{i<0} \tag{A.9}$$

If the boundary of the patch is contained with-in the concentric circle, than

$$\delta(x) = 2\pi h(x) \tag{A.10}$$

The area is determined by integration over x, where the lower limit of integration is given by

$$x_c = \frac{r - r_c}{2} \tag{A.11}$$

Thus, the area is given by

$$\text{Area} = \int_{x_c}^{R} \delta(x)\left[1 + \frac{x}{\left(R^2 - x^2\right)^{1/2}}\right]dx\,. \tag{A.12}$$

Acknowledgements

For financial support, the authors are grateful to the Office for Basic Energy Sciences of the U.S. Department of Energy and to the National Science Foundation (Grant #CTS-9530793).

References

Arakawa, T., S. N. and Timasheff. 1984. Mechanism of protein salting in and salting out by divalent cation salts: balance between hydration and salt binding. *Biochemistry* 23: 5912-5923.

Arakawa, T., and S. N. Timasheff. 1985. Theory of protein solubility. *Meth. Enzymology* 114: 49-77.

Ben-Naim, A. 1978. Standard thermodynamics of transfer, uses and misuses. *J. Phys. Chem.* 82: 792-803.

Chalikian, T. V., A. P. Sarvazyan, and L. J. Breslauer. 1994. Hydration and partial compressibility of biological compounds. *Biophys. Chem.* 51: 89-109.

Coen, C. J., H. W. Blanch, and J. M. Prasnitz. 1995. Salting-out of aqueous proteins: phase equilibria and intermolecular potentials. *AIChE J.* 41: 996-1004.

Collins, K. D., and M. W. Washabaugh. 1985. The Hofmeister effect and the behavior of water at interfaces. *Quart. Rev. Biophys.* 18: 323-421.

Connolly, M. 1993. The molecular surface package. *J. Mol. Graph.* 11: 139-143.

Curtis, R. A., A. Montaser, J. M. Prausnitz, and H. W. Blanch. 1998. Protein-protein and protein-salt interactions in aqueous protein solutions containing concentrated electrolytes. *Biotech. Bioeng.* 57: 11-21.

Eisenberg, D., and A. D. McLachlan. 1986. Solvation energy in protein folding and binding. *Nature* 319: 199-203.

Eisenhaber, F. 1996. Hydrophobic regions on protein surfaces, derivation of the solvation Energy from their area distribution in crystallographic protein surfaces. *Protein Sci.* 5: 1676-1686.

George, A., and W. W. Wilson. 1994. Predicting protein crystallization from a dilute solution property. *Acta Crsyt.* D51: 361-365.

Hermann, R. B. 1972. Theory of hydrophobic bonding. II. The correlation of hydrocarbon solubility in water with solvent cavity surface area. *J. Phys. Chem.* 76: 2754-2759.

Hofmeister, F. 1888. Zue Lehre von der Wirkung der Saltze. *Arch. Expt. Pathol. Pharmakol.* 24: 247-260.

Israelachvili, J. 1992. Intermolecular and Surface Forces: with Applications to Colloidal and Biological Systems. Academic Press, London.

Jackson, G., W. G. Chapman, and K. E. Gubbins. 1988. Phase equilibria of associating fluids, spherical molecules with multiple bonding sites. *Mol. Phys.* 65: 1-31.

Kuehner, D. E., J. Engmann, F. Fergg, M. Wernick, H. W. Blanch, and J.M. Prausnitz. 1999. Lysozyme net charge and ion binding in concentrated aqueous electrolyte solutions. *J. Phys. Chem. B* 103: 1368-1374.

McMillan, W. G., and J. E. Mayer. 1945. The statistical Thermodynamics of multicomponent systems. *J. Chem. Phys.* 13: 276-305.

Melander, W., and C. Horvath. 1977. Salt effects on hydrophobic interactions in precipitation and chromatography of proteins: An interpretation of the lyotropic series. *Arch. Biochem. Biophys.* 183: 200-215.

Munshi, C., and H. C. Lee. 1997. High-level expression of recombinant Aplysia ADP-Ribosyl Cyclase in *Pichia Pastoris* by fermentation. *Prot. Express. Purific.* 11: 104-110.

Nandi, P. K., and D. R. Robinson. 1972. The effects of salts on the free energy of the peptide group. *J. Amer. Chem. Soc.* 94: 1299-1307.

Reynolds, J. A., D. B. Gilbert, and C. Tanford. 1974. Empirical correlation between hydrophobic free energy and aqueous cavity surface area. *Proc. Natl. Acad. Sci.* 71: 2925-2927.

Ries-Kautt, M. A., and A. F. Ducruix. 1989. Relative effectiveness of various ions on the solubility and crystal growth of proteins. *J. Biol. Chem.* 264: 745-750.

Robinson, D. R., and W. P. Jencks. 1965. The effect of concentrated salt solutions on the activity coefficient of acetyltetraglycine ethyl ester. *J. Amer. Chem. Soc.* 87: 2470-2479.

Rosenbaum, D., P. C. Zamora, and C. F. Zukoski, 1996. Phase behavior of small attractive colloidal particles. *Phys. Rev. Lett.* 76: 150-153.

Sharp, K. A., A. Nicholls, R. Friedman, and B. Honig. 1991. Extracting hydrophobic free energies from experimental data: relationship to protein folding and theoretical models. *Biochemistry* 30: 9686-9697.

Shugar, D. 1952. The measurement of lysozyme activity and the ultra-violet inactivation of lysozyme. *Biochim. Biophys. Acta* 8: 302-309.

Sinanoglu, O. 1968. Solvent effects on molecular association. *In* Molecular Associations in Biology. B. Pullman, editor. Academic Press, New York.

Sophianopoulus, A. J., C. K. Rhodes, D. N. Holcomb, and K.E. van Holde. 1962. Physical studies of lysozyme I , characterization. *J. Biol. Chem.* 237: 1107-1112.

Stockmayer, W. H. 1950. Light scattering in multi-component solutions. *J. Chem. Phys.* 18: 58-61.

ten Wolde, P. R.., and D. Frenkel. 1997. Enhancement of protein crystal nucleation by critical density fluctuations. *Science* 277: 1975-1978.

Verwey, E. J. W., and J. T. G. Overbeek. 1948. Theory of the Stability of Lyophobic Colloids. Elsevier Publishing Company, Amsterdam.

Vilker, V. L., C. K. Colton, and K.A. Smith. 1981. Osmotic pressure of concentrated protein solutions: the effect of concentration and pH in saline solutions of bovine serum albumin. *J. Colloid Int. Sci.* 79: 548-566.

von Hippel, P. H., and T. Schleich. 1969. Ion effects on the solution structure of biological macromolecules. *Acc. Chem. Res.* 2: 257-265.

Wang, H., and A. Ben-Naim. 1997. Solvation and solubility of globular proteins. *J. Phys. Chem. B* 101: 1077-1086.

Wertheim, M. S. 1984. Fluids with highly directional attractive forces. I. Statistical thermodynamics. *J. Stat. Phys.* 35: 19-34.

Net Charge, pH 7	8
Net Charge, pH 4.5	12
H/k_BT	3.0
Effective spherical diameter (Å)	34.4
f_a	0.49
f_p	0.51
Area Hydrophobic Patch (Å^2)	97.0

Table 1: Parameters used in potential of mean force calculations. The net charge parameters are given in Kuehner et al. (1999). The effective spherical diameter is determined from lysozyme crystal dimensions. f_a and f_p are the fractional coverages of nonpolar and polar groups, respectively, for native lysozyme.

List of Figures:

Figure 1: The solvation force is described by a surface free energy multiplied by the surface area buried by the interaction. This is approximated by the spherical cap area of the proteins colored in dark grey. The surface-to-surface cut-off separation, r_c, is approximated by a solvent diameter. The combined areas of the spherical cap regions enclosed by the box is given by $A(r) = 2\left[\int_0^{\theta} \frac{\pi d_2^2}{2} \sin\theta' d\theta'\right] = \pi d_2^2 - \pi r d_2 + \pi r_c d_2$ where d_2 is the diameter of the protein, θ is the solid angle corresponding to the boundary of the spherical cap and $\cos\theta = \frac{r - r_c}{2R}$.

Figure 2: The mutated residue is modeled as a circular patch on the surface of the sphere. The patch-patch interaction is given by the nonpolar surface free energy multiplied by the surface area of the patch that is with-in a cut-off separation, r_c, of the second sphere. Here, this area is given by the total area of the two patches that is enclosed by the box. See text for description of the angles of rotation, α_1, α_2, φ_1, and φ_2. r_c is the cut-off surface-to-surface separation approximated as a solvent diameter and d_2 is the protein diameter.

Figure 3: On the left is the space-filling structure of D101F lysozyme, where the mutated residue is shown in dark grey. The blow-up of the region is shown on the top right and the analagous representation for the native form is shown on the bottom right.

Figure 4: Experimental B_{22} for lysozyme in solutions of sodium chloride or ammonium sulfate versus salt molality.

Figure 5: Surface free energy of lysozyme determined from fitting B_{22} to potential-of-mean-force model described by Eq. 6, with $H = 3.0\ k_BT$, $r_c = 3$ Å.

Figure 6: Experimental B_{22} for D101F lysozyme or for native lysozyme in solutions of sodium chloride versus salt molality.

Figure 7: Predicted light-scattering data for D101F lysozyme using Wertheim's model with full expression from perturbation theory or osmotic virial expansion truncated at second virial coefficient. The fraction of unbonded molecules is shown in the inset.

Figure 8: Hydrophobic surface free energy for D101F lysozyme calculated from Wertheim's model and from the patch model versus salt molality.

Figure 9: Apparent molecular weights for D101F lysozyme in solutions of ammonium sulfate or sodium chloride versus salt molality.

Figure 10: Experimental values of B_{22} for native lysozyme or for D101F lysozyme in solutions of ammonium sulfate versus salt molality.

Figure 11: Experimental light-scattering data for D101F lysozyme in 1.0 molal ammonium sulfate plotted with the best fit to Wertheim's model.

Figure 12: Surface free energy calculated from Wertheim's model for D101F lysozyme in solutions of ammonium sulfate, pH 7 versus salt molality.

Figure 13: The patch-patch interaction is calculated by summing up the area of both patches that is with-in the cut-off separation r_c given by the area enclosed in the box. The variables are explained in Appendix A. The inset shows the coordinate system for the calculation along with the one denoting the orientation of the patch given by the primed variables.

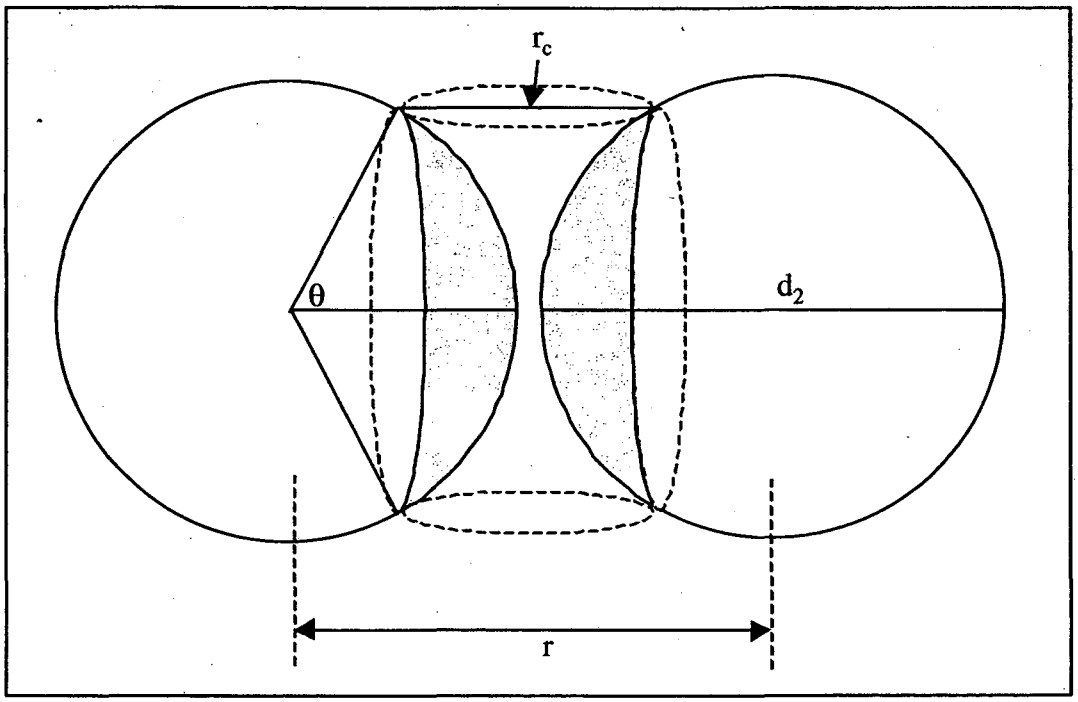

Fig 1

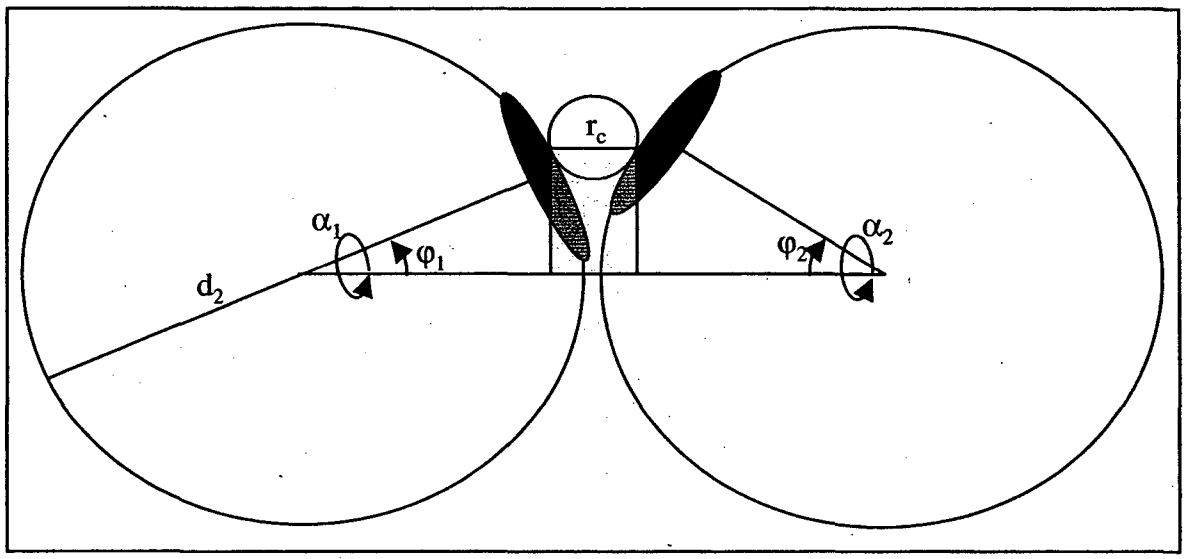

Fig 2

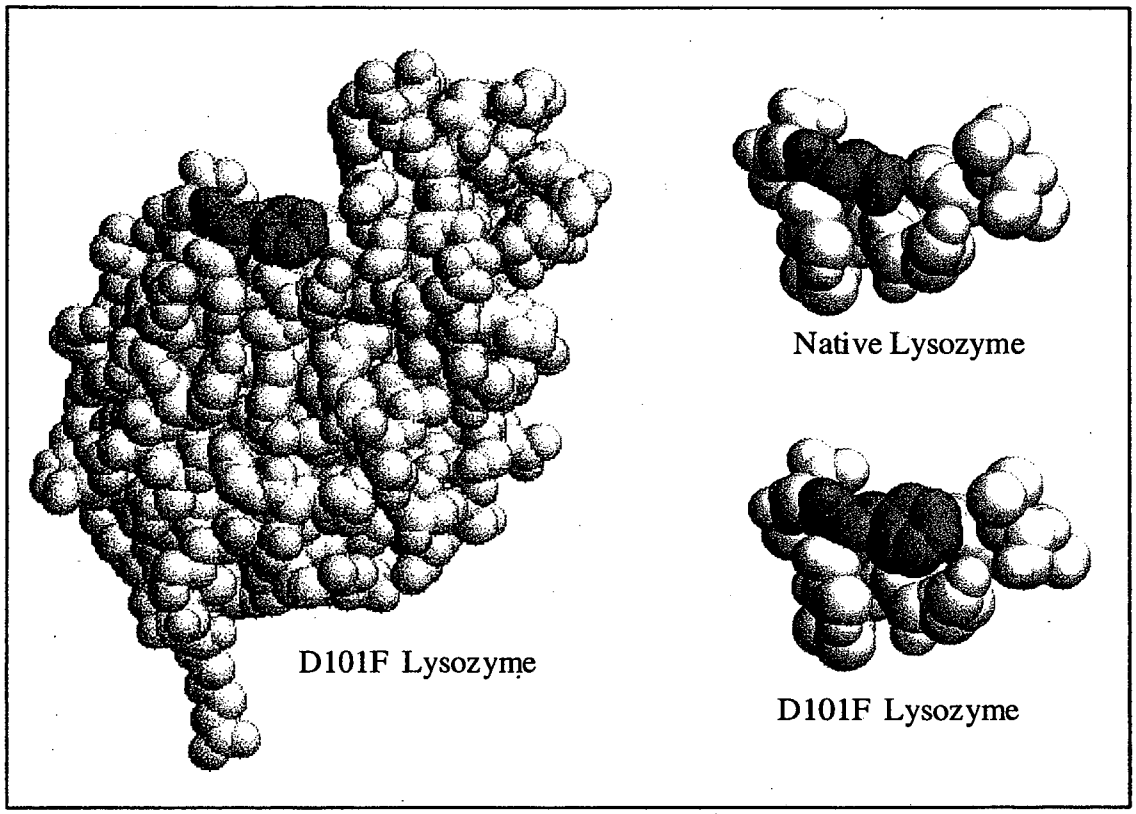

Fig 3

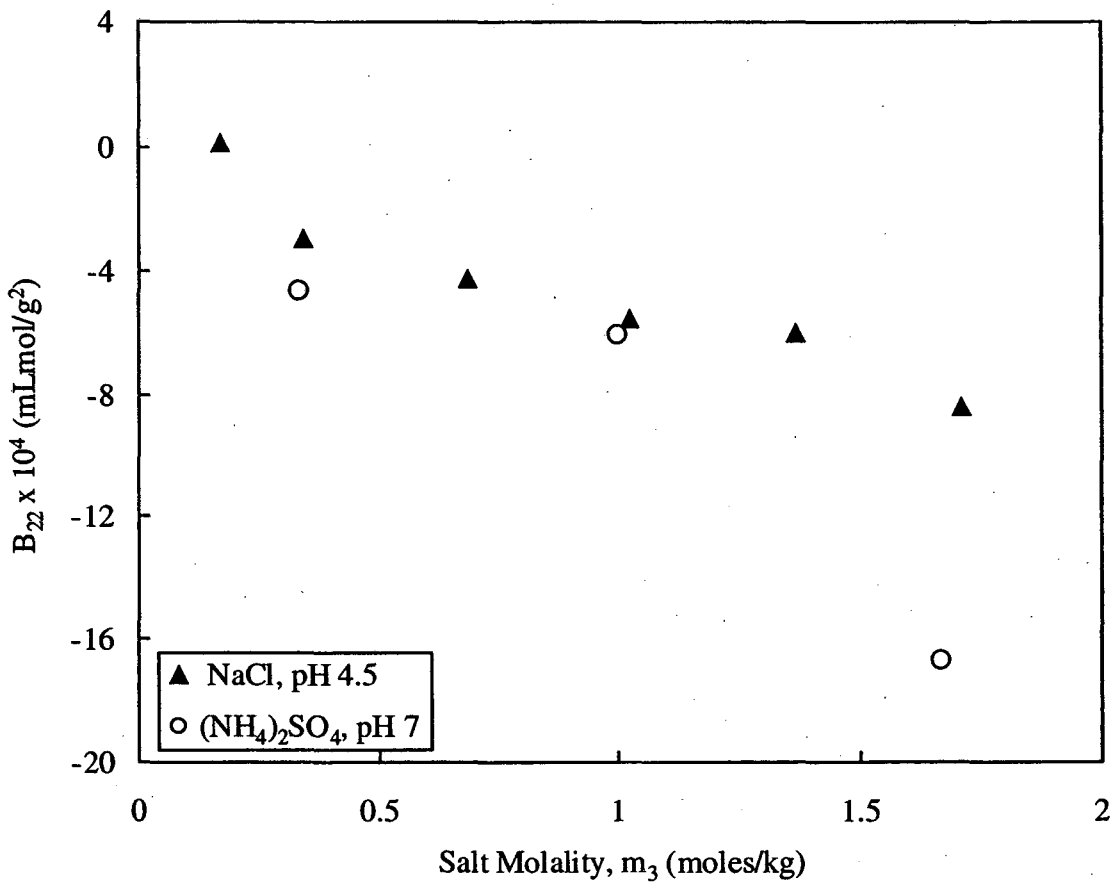
4
0
-4
-8
-12
-16
-20
B_{22} x 10^4 (mLmol/g^2)
NaCl, pH 4.5
$(NH_4)_2SO_4$, pH 7
0
0.5
1
1.5
2
Salt Molality, m_3 (moles/kg)

Fig 4

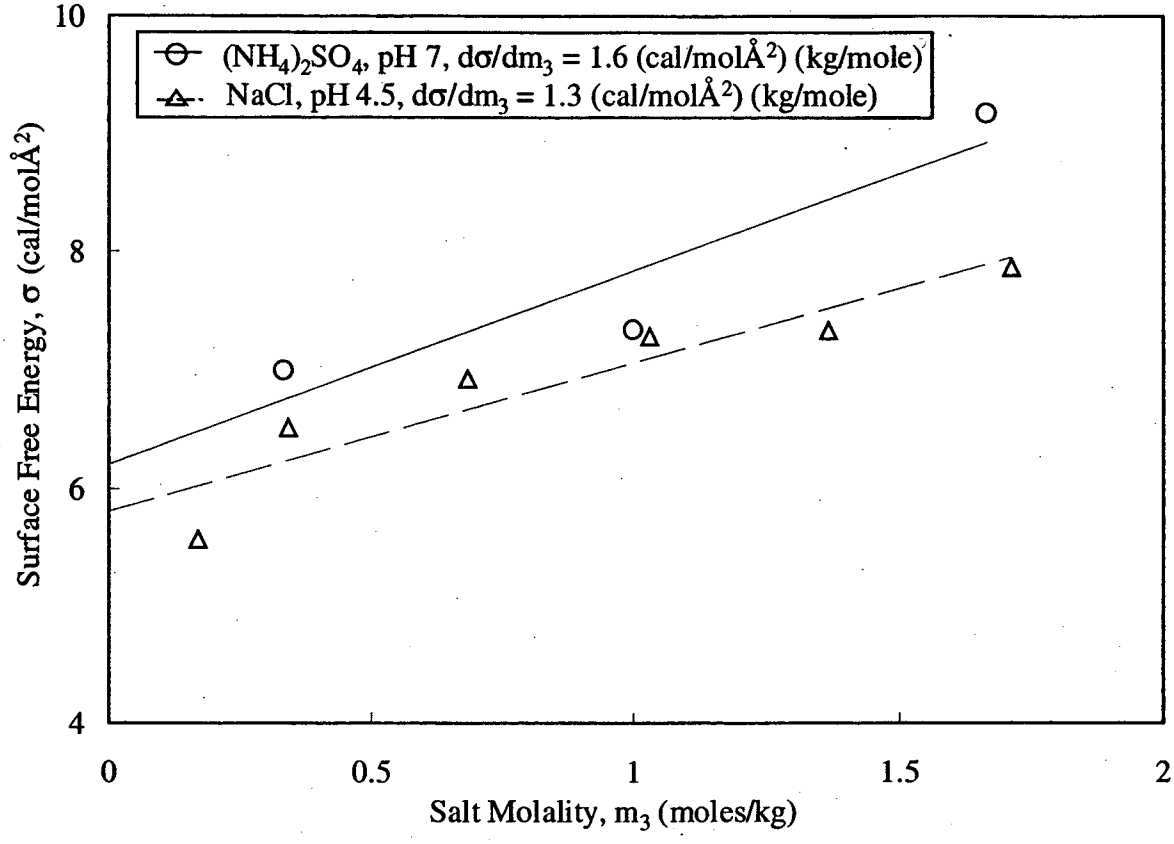
(NH4)2SO4, pH 7, dσ/dm3 = 1.6 (cal/molÅ2) (kg/mole)
NaCl, pH 4.5, dσ/dm3 = 1.3 (cal/molÅ2) (kg/mole)
Surface Free Energy, σ (cal/molÅ2)
10
8
6
4
0
0.5
1
1.5
2
Salt Molality, m3 (moles/kg)

Fig 5

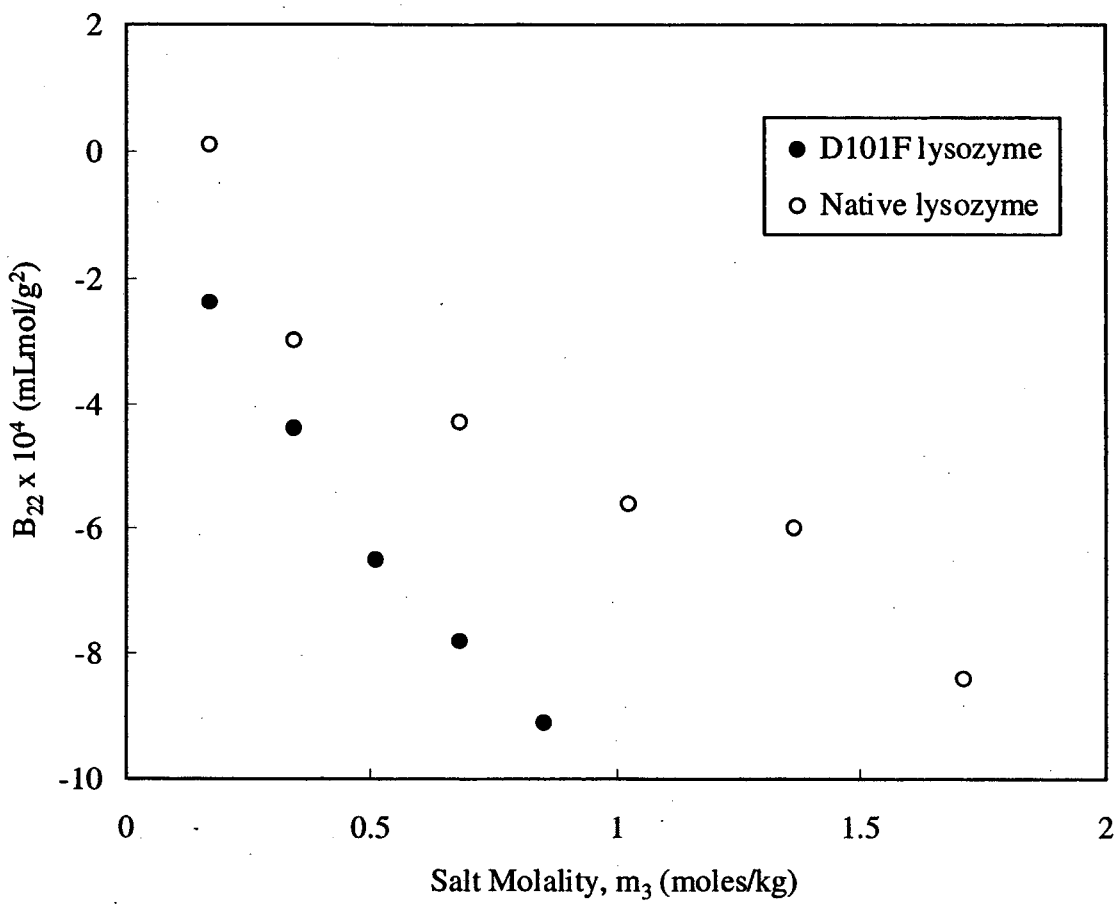
2
0
-2
-4
-6
-8
-10
0
0.5
1
1.5
2
B_{22} x 10^4 (mLmol/g^2)
Salt Molality, m_3 (moles/kg)
D101F lysozyme
Native lysozyme

Fig 6

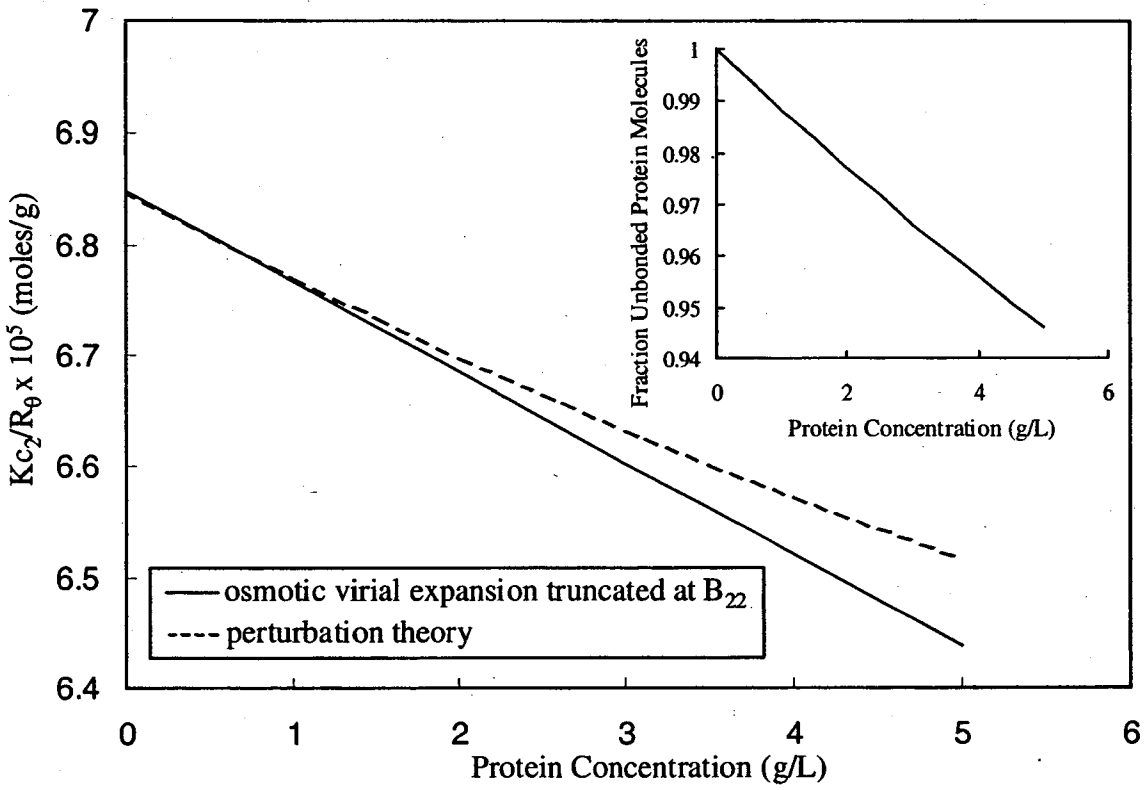
7
6.9
6.8
6.7
6.6
6.5
6.4
Kc_2/R_θ x 10^5 (moles/g)
0
1
2
3
4
5
6
Protein Concentration (g/L)
osmotic virial expansion truncated at B_{22}
perturbation theory
Fraction Unbonded Protein Molecules
1
0.99
0.98
0.97
0.96
0.95
0.94
0
2
4
6
Protein Concentration (g/L)

Fig 7

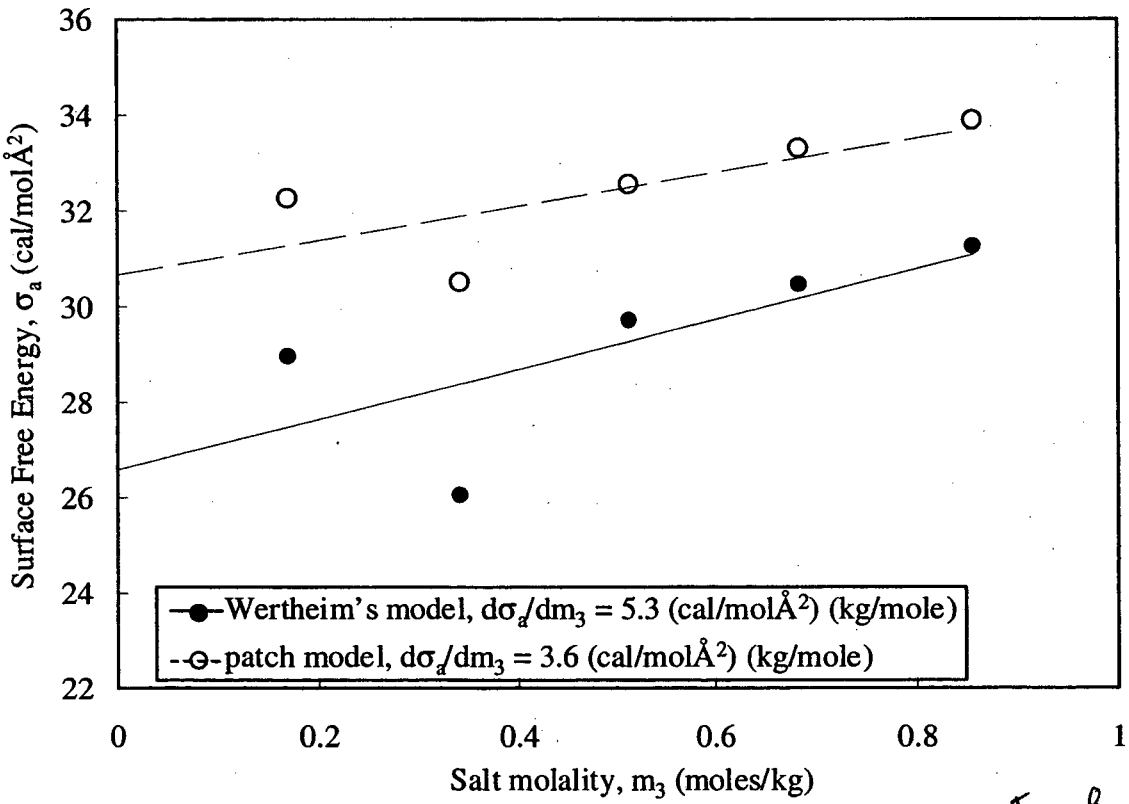
36
34
32
30
28
26
24
22
Surface Free Energy, σ_a (cal/molÅ^2)
0
0.2
0.4
0.6
0.8
1
Salt molality, m_3 (moles/kg)
Wertheim's model, $d\sigma_a/dm_3$ = 5.3 (cal/molÅ^2) (kg/mole)
patch model, $d\sigma_a/dm_3$ = 3.6 (cal/molÅ^2) (kg/mole)

Fig 8

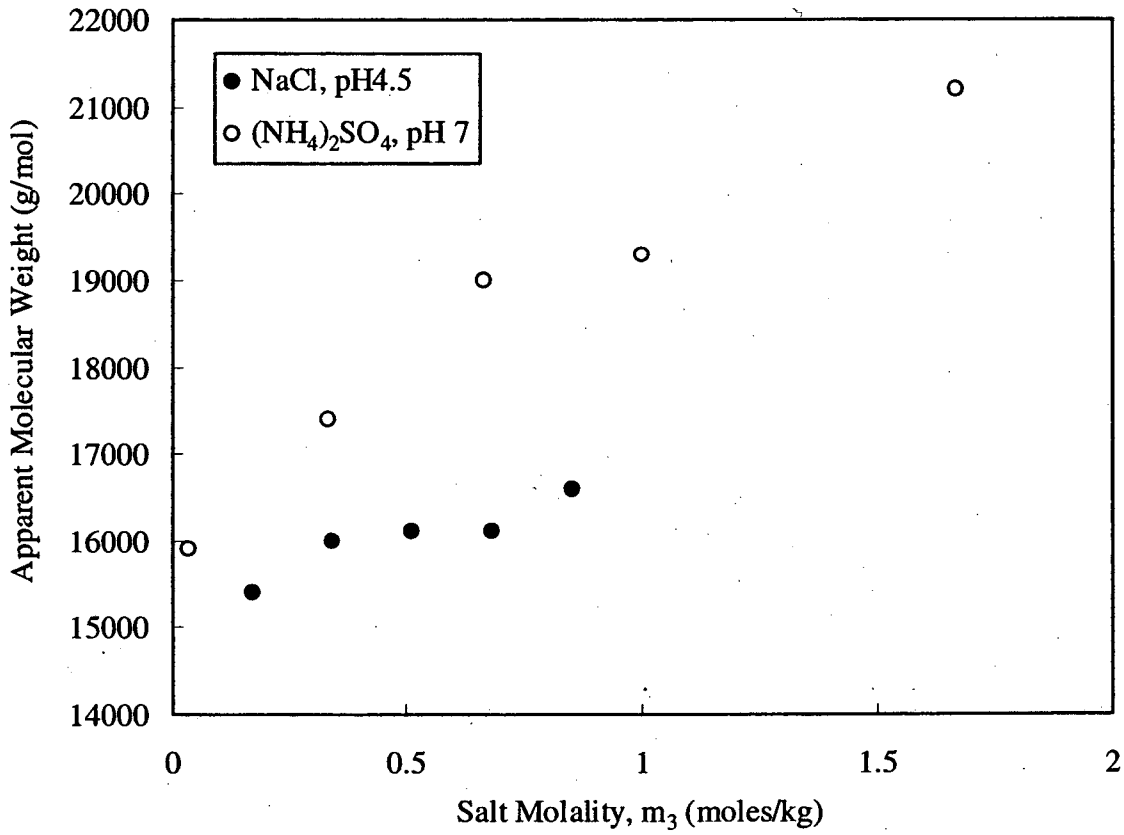
22000
21000
20000
19000
18000
17000
16000
15000
14000
Apparent Molecular Weight (g/mol)
NaCl, pH4.5
(NH4)2SO4, pH 7
0
0.5
1
1.5
2
Salt Molality, m3 (moles/kg)

Fig 9

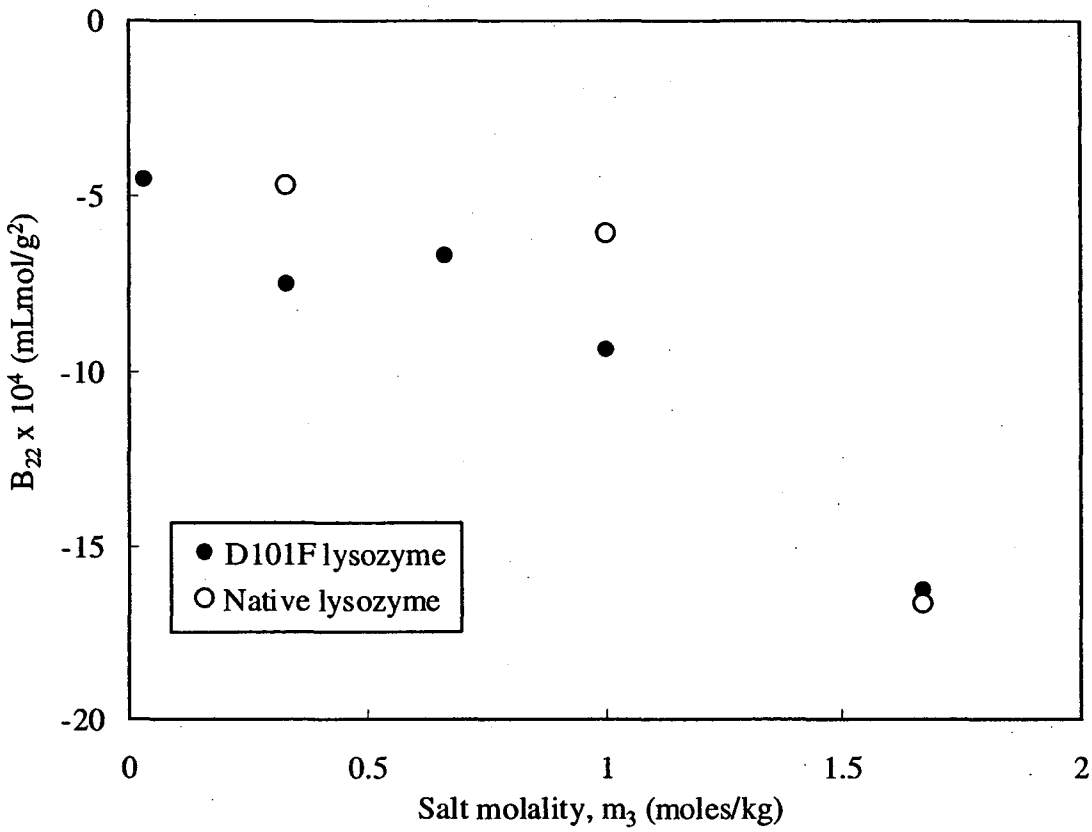
0
-5
-10
-15
-20
B_{22} x 10^4 (mLmol/g^2)
D101F lysozyme
Native lysozyme
0
0.5
1
1.5
2
Salt molality, m_3 (moles/kg)

Fig 10

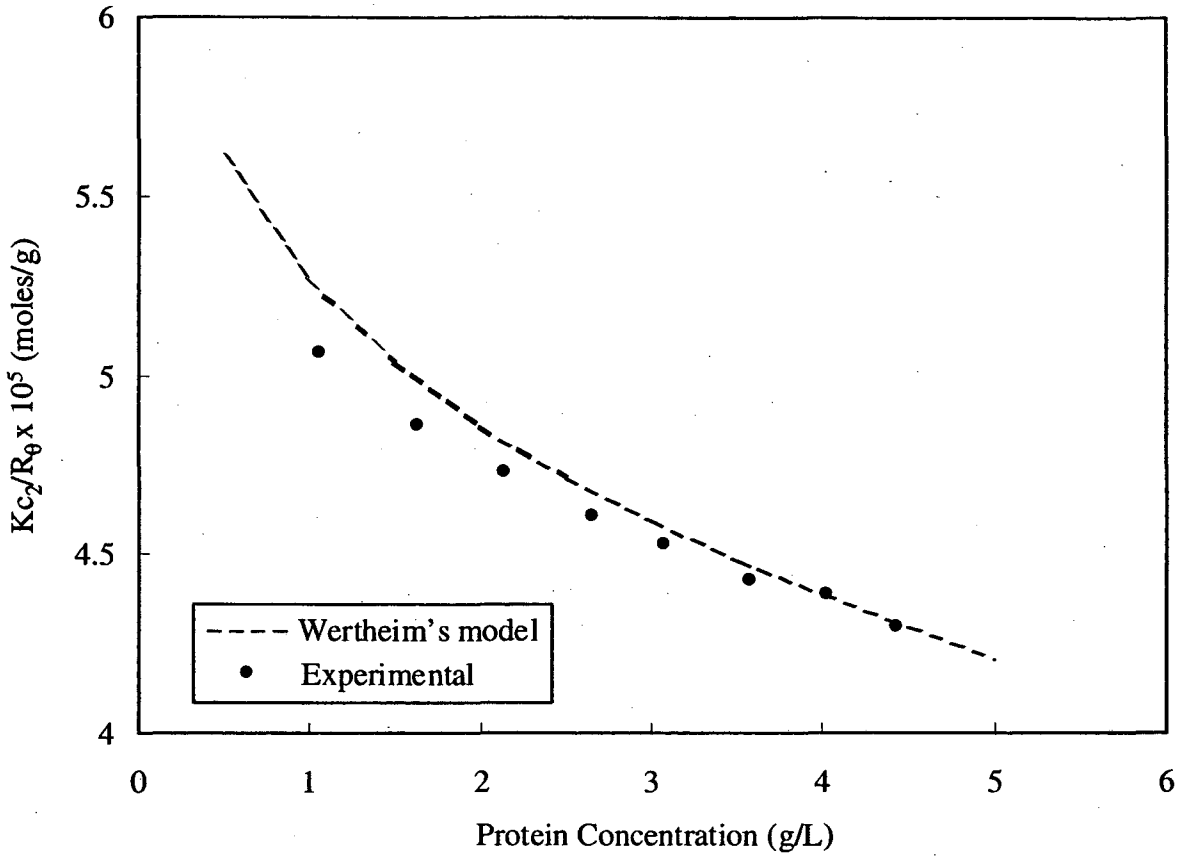
6
5.5
5
4.5
4
0
1
2
3
4
5
6
Kc_2/R_θ x 10^5 (moles/g)
Protein Concentration (g/L)
Wertheim's model
Experimental

Fig 11

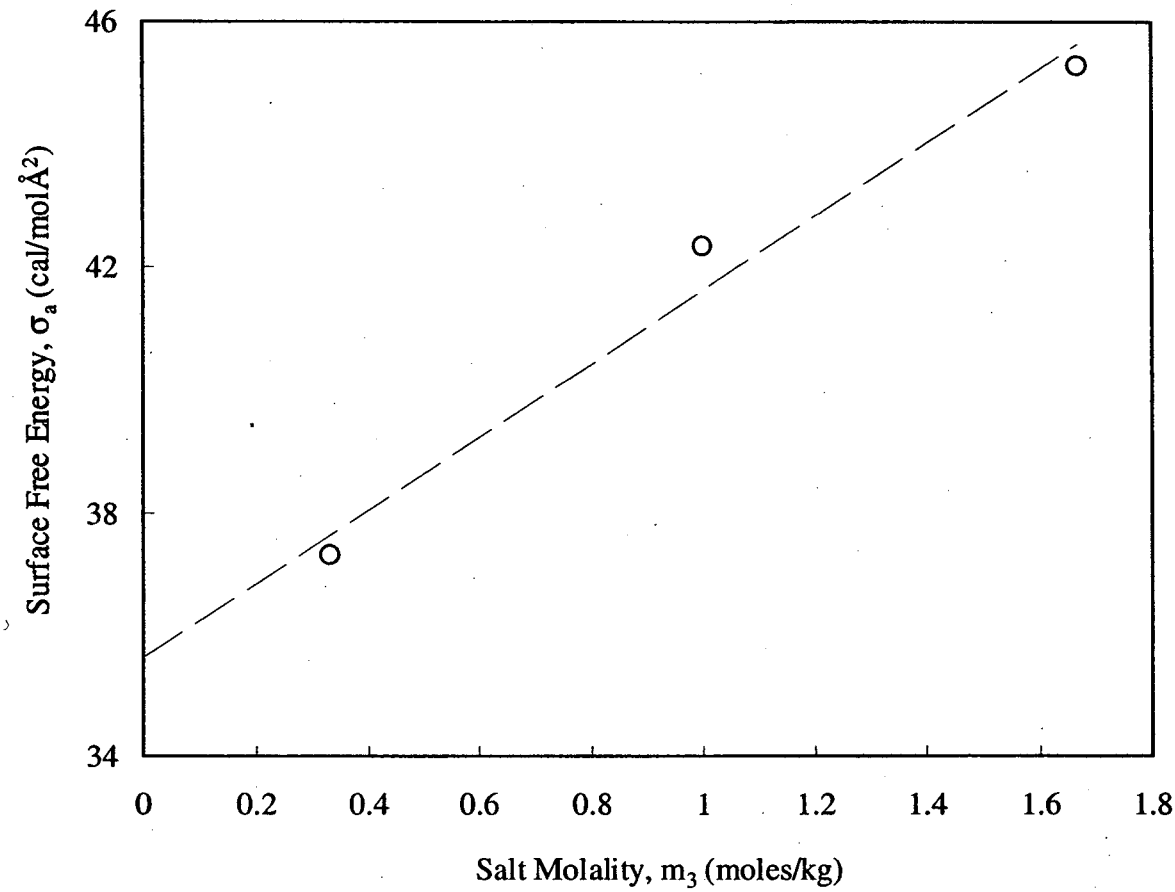
46
42
38
34
0
0.2
0.4
0.6
0.8
1
1.2
1.4
1.6
1.8
Surface Free Energy, σ_a (cal/molÅ^2)
Salt Molality, m_3 (moles/kg)

Fig 12

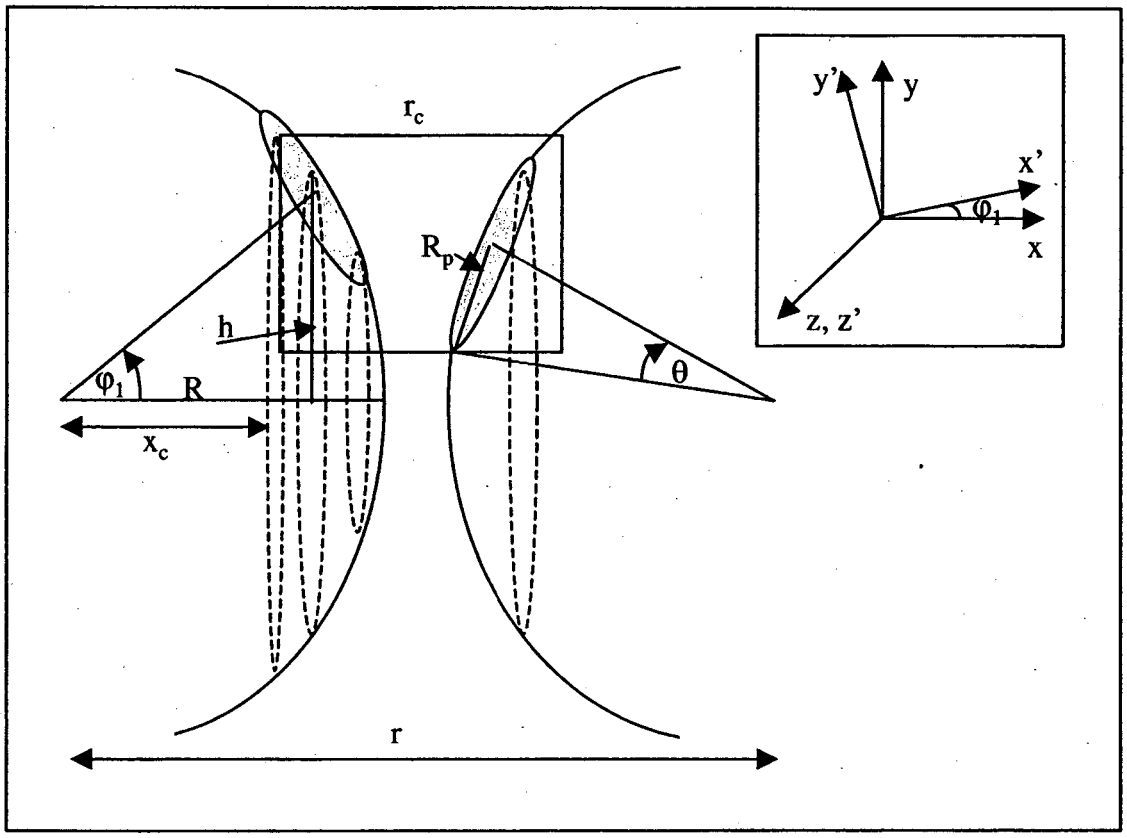

Fig 13

Ernest Orlando Lawrence Berkeley National Laboratory
One Cyclotron Road | Berkeley, California 94720

Prepared for the U.S. Department of Energy under Contract No. DE-AC03-76SF00098